Article

Laboratory-synthesized biogenic silver nanoparticles (AgNPs) with potential therapeutic applications

Fatima M. Hamed [1], Hanan A. Ghozlan [1, *], Soraya A. Sabry [1], Samia S. Abouelkheir [2]

[1] *Faculty of Science, Alexandria University, Moharrem Bey, 21511 Alexandria, Egypt.*
[2] *National Institute of Oceanography and Fisheries (NIOF), Alexandria, Egypt.*
[*] *Correspondence Address:*

Hanan A. Ghozlan: Professor of Microbiology, Faculty of Science, Alexandria University, Egypt, Mobile: 00201000160509, E. mail address: Ghozlan.hanan@alexu.edu.eg ORCID: https://orcid.org/0000-0002-7775-1369.

ABSTRACT: This research was planned to isolate a marine bacterium that is able to biosynthesize silver nanoparticles to be used for therapeutic applications. The environmentally friendly production of nanoparticles from biological sources is frequently simple, inexpensive, and free of hazardous chemicals. Silver nanoparticles (AgNPs) are part of a new class of biomaterials that is being created more and more for use in scientific and medical endeavours. Given how important the biological system is, it is essential to have a basic understanding of how inorganic nanoparticles affect cellular development and function. Resazurin, a rapid screening assay, was applied to evaluate the antibacterial effects of the synthesized AgNPs against the pathogenic microbes. The 3-[4,5-dimethylthiazol-2-yl]-2,5 diphenyl tetrazolium bromide (MTT) assay was utilized to test silver nanoparticles for cell cytotoxicity and anticancer activity. Silver nanoparticles (AgNPs) were tested for wound healing effects using a scratch assay on a human epithelial cell line (WISH-CCL-25). *Halomonas* sp. FSSH, among many isolates successfully biosynthesized silver nanoparticles with interesting properties. The present finding revealed that supernatant of *Halomonas* sp. FSSH could be effectively used as a reducing agent for the green production of AgNPs. These AgNPs are considered efficient antimicrobial, anticancer, and wound-healing agents without cytotoxic effects.

1. INTRODCTION

Green nanotechnology is trending worldwide and has recently made a significant contribution, especially in biomedical applications due to the sustainable growth of human society. Owing to its unique properties, nanotechnology offers solutions to improve conventional technologies. The green production of nanoparticles from biological sources is frequently simple, cost-effective, and avoids the use of hazardous chemicals. This may lead to biologically active, homogeneous (in shape and size) products. Green synthesis is less harmful to human wellness and the surrounding environment compared to common chemical and physical methods [1-3]. The greatest microbial ecology on Earth is found in the marine environment. Therefore, microbial diversity, particularly marine bacteria, is a valuable and promising natural source for enzymes of industrial significance and bioactive metabolites. More than 99% of these bacteria are uncultured, and thus they are largely unknown to science [4]. The use of man-made metal nanoparticles (MNPs) in medicine is linked to highly complex nanostructures that will let doctors get close to the human body at the cellular and molecular levels. With the design of specific nanostructures, these can be used as new diagnostic and treatment methods. Numerous medical uses of nanoparticles exist, such as their utilization as drug delivery systems, radiosensitizers in radiation or proton treatment, and in the field of bioimaging [5].

Nowadays, deadly diseases such as bacterial infections and cancer are the cause of many deaths. Pathogenic gram-positive and negative bacteria trigger infection in many areas. According to the WHO report, liver cancer has become one of the lethal agents in the world, and various therapy methods such as surgery and chemotherapy are also not suitable for everyone because of the great tissue damage they cause [6]. Metal nanoparticles can be used as bactericides and fungicides due to their exceptional properties, such as their enormous surface-to-volume ratio and good biocompatibility [7]. They are known to have non-specific bacterial toxicity mechanisms, i.e., they do not bind to specific receptors in the microbial cell. Unlike antibiotics, this property may not lead to the emergence of resistance [8]. While the largest organ in the human body is the skin, it serves important functions, the most important of which is the protection of internal organs and immune defence. Any disruption of normal tissue structure and function, either by surgery or trauma, may lead to pathological changes in the body. Few studies were available regarding the role of AgNPs in skin wound healing [9, 10].

In addition, poor wound healing puts more strain on the patient and the healthcare system. So, any technology that improves the healing process has the potential to save billions in annual health care costs and preserve the patient's quality of life by reducing fluid loss [11].

In this work, it is aimed to isolate a marine bacterium that has the ability to form silver nanoparticles and examine the potential antimicrobial activity, cytotoxicity on rabbit leukocyte cells, the potential anticancer agent in cancer therapy on the human liver cancer cell line (HepG2), and the healing process of skin wounds on human epithelial cell line (WISH).

2. Material and Methods

2.1. Chemicals and supplies

Silver nitrate ($AgNO_3$) was purchased from Alpha Chemika Co., Ltd. Nutrient broth (NB) was obtained from BioLab Co., Ltd. Nutrient agar (NA) was purchased from Biolife Co., Ltd. All chemicals and analytical reagents were used without further purification. Throughout the experiments, distilled and seawater were used.

2.2. Sample collection

Sediment samples were collected from Ain El-Sokhna, Egypt. Ain El-Sokhna belongs to the Suez Governorate on the western shore of the Red Sea's Gulf of Suez, approximately 120km East of Cairo. The climate of Ain El-Sokhna is a hot desert climate ranging from 8 to 40°C [12]. The three collected samples were transferred into a sterilized container and immediately transported to the microbiology laboratory at the National Institute of Oceanography and Fisheries (NIOF) in an ice box for bacterial enrichment and isolation.

2.3. Isolation of bacteria

One gram of sediment from each sample separately was mixed with 100ml of nutrient broth at pH 7, and then incubated at 37°C for 48h. Pure colonies were isolated, selected, and tested for primary AgNPs biosynthesis. The promising isolate was considered a potential candidate and was tested for Gram reaction [13], blood hydrolysis [14], growth on MacConkey agar plate [15], and potassium hydroxide (KOH) test [16].

2.4. Genotypic characterization

Genomic DNA was extracted from the pure selected isolate, and the 16S rRNA gene was amplified by polymerase chain reaction (PCR) using the universal primer pair 16S rRNA. The amplicons were tested using electrophoresis [17]. The PCR product was sequenced using the sequencing facility provided by Sigma Scientific Services-Egypt.

2.5. Biosynthesis of silver nanoparticles (AgNPs)

The glycerol-stocked bacterial cells were used to prepare a seed culture. Cells are inoculated into 100 mL of Nutrient Broth (NB) medium in a 250 mL Erlenmeyer flask and shaken at approximately 120 rpm overnight at 37°C for activation. The freshly prepared seed culture was used as inoculum (2%, $OD_{600nm} \approx 0.5$) for a 250 mL Erlenmeyer flask containing 100 mL of NB (pH 7.0). Then the flasks were incubated at 37°C at 120 rpm for 24h, until OD_{600} reached 1. The cell-free supernatant was obtained by centrifugation at 5000 rpm for 15 min, and then 100 mL of the supernatant was mixed with 100 mL of $AgNO_3$ solution (40 mM) and incubated at 37°C in a shaker incubator at 200 rpm for 10 min [18, 19]. The produced

nanomaterial was centrifuged at 5000 rpm for 15 min to achieve absolute separation. The supernatant was decanted off to collect the pellet, which was washed three times with distilled water to efficiently separate the nanoparticles. The nanoparticles were then dried in a 50°C oven for 24h and used for further research.

2.6. Characterization of AgNPs

The typical ultraviolet-visible (UV-Vis) absorption spectra of AgNPs were measured by a UV-Vis spectrophotometer (Chrom Tech, model CT-2200M Taiwan). Transmission electron microscopy (TEM) images of AgNPs were observed on the JSM-1400 plus microscope with an accelerating voltage of 80 kV (JEOL, Japan). Images from a JSM-IT200 scanning electron microscope (SEM) were obtained. Energy-dispersive X-ray (EDX) equipped with a scanning electron microscope (JEOL, Japan) operated at 20kV. X-ray powder diffraction (XRD) patterns were obtained using a Bucker D2-phaser instrument (Bruker, Germany) operated at 30KV with Cu Kα λ=1.54184Å radiation. Fourier transform infrared spectroscopy (FTIR) was recorded from 500-4000cm^{-1} with samples prepared as KBr pellets (Bruker, Germany). At 25°C, the particle size and zeta potential of AgNPs were measured using the Zeta Nanosizer instrument (Malvern, UK). The preparation of samples for the previously mentioned tests was carried out following the manufacturer's instructions at the Central Laboratories, Faculty of Science, and Faculty of Pharmacy, Alexandria University.

2.7. Antimicrobial activity and Minimum Inhibitory Concentration (MIC) determination for AgNPs via a Resazurin-based turbidimetric assay

Resazurin, a rapid screening assay, was used to test the antibacterial activities of the synthesized AgNPs against the following microbes: *Escherichia coli* (*E. coli*) (ATCC: 8739), *Klebsiella pneumonia* (*K. pneumonia*) (ATCC: 13883), *Pseudomonas aeruginosa* (*P. aeruginosa*) (ATCC: 15442), *Vibreo parahemolyticu* (*V. parahemolyticus*), *Enterococcus faecalis* (*E. faecalis*) (ATCC: 29212), *Staphylococcus aureus* (*S. aureus*) (ATCC: 25923), *Bacillus subtilis* (*B. subtilis*) (ATCC: 6633), and *Candida albicans* (*C. albicans*) (ATCC: 10231) was determined according to methodology of Miranda and his colleagues [20] with some modifications. Five µL of microbial suspension whose turbidity was adjusted to a 0.5 McFarland standard were placed in 96 wells. Silver nanoparticles (95 µL) were added at the following concentrations: 1000, 500, 250, 125, 62.5, and 31.25 µg/100 µL. A microbe without AgNPs was used as a positive control, while two negative controls were prepared using AgNPs in distilled water and NB. Where column 1 represents control containing water with AgNPs, column 2 contains NB with AgNPs, and columns 3-10 contain tested pathogens with different concentrations of AgNPs, the upper row represents the higher concentrations. Resazurin indicator solution (5 µL of 0.0125 mM) was transferred to each well after overnight incubation at 37°C and kept for another 4h. Changes in colour were observed and recorded. The lowest concentration prior to colour change was considered the minimum inhibitory concentration (MIC) [21, 22].

2.8. Silver nanoparticles' cell cytotoxicity and anticancer activity

The 3-[4,5-dimethylthiazol-2-yl]-2,5-diphenyl tetrazolium bromide (MTT) assay was used to test silver nanoparticles for

cell cytotoxicity and anticancer activity. The assay is a common method for determining the number of viable cells based on the activity of succinate dehydrogenase. Cell cytotoxicity was determined on rabbit leukocyte cells, while anticancer activity was determined on a human liver cancer cell line (HepG2-HB-8065). In a 96-well plate, serial dilution of the AgNPs was prepared using culture medium. The treatment was done in triplicate, and two control columns (media only) were maintained in a 5% CO_2 incubator at 37°C for 24 h. The plate was measured using the MTT assay on microplate ELISA reader [23-25]. The percentages of cytotoxicity (viability) and anticancer (inhibition) were calculated according to the following equation:

$$MTT\% = 100 - \left(\frac{Abs.Control - Abs.Treatment}{Abs.Control} \right) \qquad (1)$$

where MTT% is the percentage of cell viability for cytotoxicity and percentage of cell inhibition for anticancer. Abs. Control and Abs. Treatment are absorbance of control and treatment, respectively.

2.9. Wound healing assay

Silver nanoparticles (AgNPs) were tested for wound healing effects using a scratch assay on a human epithelial cell line (WISH-CCL-25). This is a simple, economical, and well-developed method to measure two-dimensional cell migration *in vitro* [26]. Data analysis was done using the following equation:

Wound closure presentage =

$[(Wound\ Length_{0\ Hour} - Wound\ Length_{24\ Hours})/Wound\ Length_{0\ Hour}]$

$\times \mathbf{100} \qquad (2)$

2.10. Statistical analysis

All investigations were performed in three replicates, and the results were statistically analyzed and implemented using Origin Pro 8.1 Statistical Software. The data were analyzed using ANOVA. The data were carried out based on the values, which were expressed by means ± SE. The significant values were determined at a P-value < 0.05

3. Results

3.1. Screening for culture supernatants-mediated synthesis of silver nanoparticles

In this study, five isolates from marine sediments in Ain El-Sokhna, Egypt, were isolated, purified, and investigated visually and by using UV-visible spectrophotometer for the synthesis of AgNPs. Results showed that only two isolates (F8 and F9) were capable of changing the colour from colourless to dark brown. Only isolate F8 had the highest surface plasmon resonance absorption peak at 400nm (**Figure 1**); therefore, it was selected for further investigation.

3.2. Characterization of the most promising isolate

The most promising AgNPs-producing bacterium isolate F8 was recovered on nutrient agar plate (**Figure 2a**). The morphological characteristics of colonies showed creamy colour, regular margin, convex, mucoid configuration (**Figure 2a**). **Figure 2b** showed that the cells are Gram-negative rods occurring singly. The KOH test confirmed that the isolate is Gram negative [16] (**Figure 2c**). On blood agar plates, isolate F8 showed no hemolysis (**Figure 2d**), indicating the isolate's inability to destroy red blood cells [14].

The isolate also did not show a fermentation reaction on MacConkey agar, indicating non-lactose-fermenting colonies [15] (**Figure 2e**).
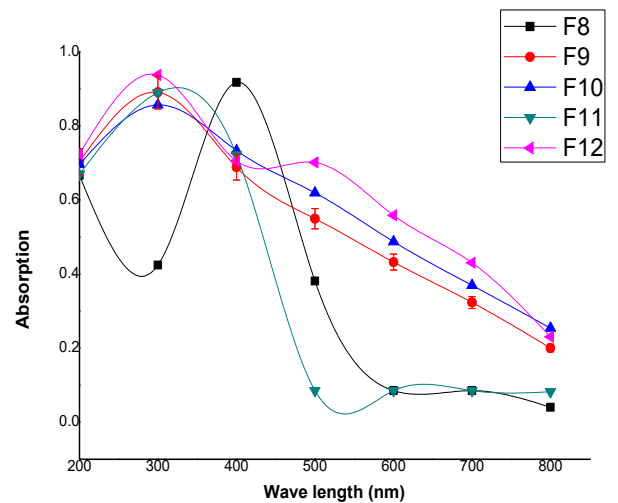
Figure 1. The UV-Vis absorption spectra of AgNPs synthesized by five bacterial isolates
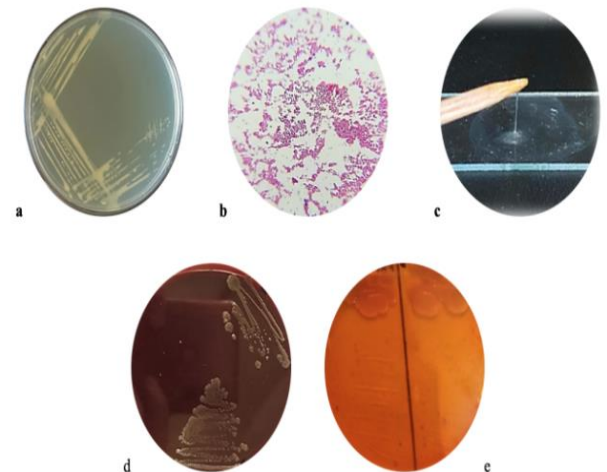
Figure 2. Isolate F8 characterization: colonies on NA plates after 24h of incubation at 37°C (a); light micrograph of Gram stain (b); KOH test (c); growth on blood agar (d); growth on MacConkey agar (e)

In a sequential step, it was necessary to identify the promising isolate (F8) by amplifying the 16S rRNA gene. The amplified fragments (1474 bps) were sequenced. The sequence of the 16S rRNA gene in isolate F8 was 97% the same as the sequence of *Halomonas denitrificans* (NR_042491.1). The 16S rRNA gene sequence was deposited as OP716688 in GenBank, designated as *Halomonas* sp. FSSH, and classified as a member of the genus *Halomonas*, family Halomonadaceae, order Oceanospirillaes, class γ-Proteobacteria, phylum Pseudomonadota. The phylogenetic bond between the amplified 16S rRNA sequence and its nearby relatives is summarized in the phylogenetic tree in **Figure 3**.
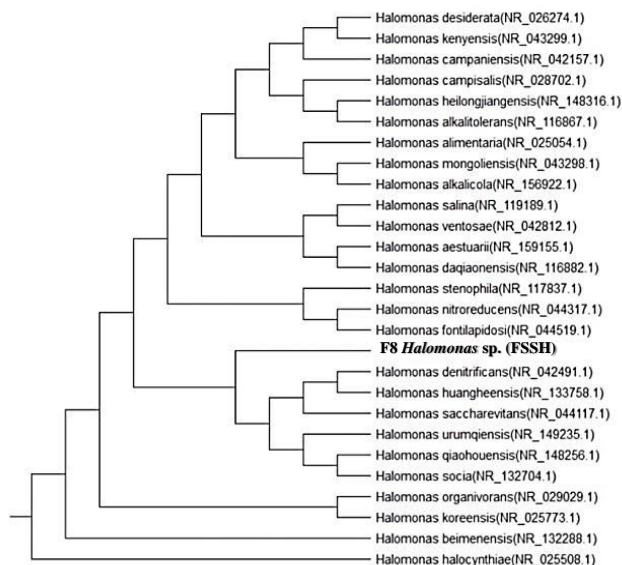
Figure 3. Phylogenetic tree of isolate F8 based on 16S rRNA sequence analysis among closely related *Halomonas* species

The identified marine bacterium *Halomonas* sp. FSSH was cultured in nutrient broth (NB) at pH 7 and 37 °C under shaken growth conditions for 24 h. Around 100 ml of the supernatant were used to synthesize silver nanoparticles (AgNPs) that seemed as a dark brown powder distributed in solution (**Figure 4a**). The nanoparticles produced were washed, purified, and dried for characterization.

3.3. Biogenic silver nanoparticles (AgNPs) characterization

Several analytical techniques were applied to evaluate the bio-manufactured AgNPs, including UV-vis spectroscopy. The UV/Vis spectrum of the colloidal solution of the synthesized AgNPs showed a strong, conspicuous, characteristic spectral absorption peak at 400 nm (**Figure 4a**), confirming its presence. The formation of the AgNPs during the reduction process is indicated by a change in the colour of the $AgNO_3$ from colourless to dark brown (**Figure 4a**). According to TEM and SEM data analyses, the biosynthesized AgNPs are evenly distributed and have a spherical shape with an average size ranging from 15.69 to 133.78nm (**Figure 4b** left) and 18.30 to186.8 nm (**Figure 4b** right), respectively. By using EDX analysis, the strong absorption peak at 3keV in the metallic silver region was observed as confirmation for the AgNPs

synthesis. A trace of elements in the form of peaks was detected together with silver ions by the EDX pattern. These elements were carbon (C) (11.46%), boron (B) (11.77%), alminium (Al) (0.80%), and chlorine (Cl) (17.58%), together with metallic silver (**Figure 4c**). The XRD pattern of AgNPs showed peaks at 2θ of 38.175º, 44.370º, 64.553º, and 77.537º, which correspond to the (111), (200), (220), and (311) levels, respectively (**Figure 4d**). The crystal structure of the produced AgNPs is evident from these diffraction patterns that confirm the AgNPs have a face-centered cubic structure and also confirm the crystalline nature of AgNPs. The calculated particle size of AgNPs using the Scherrer equation was approximately 19.11 nm. Various bands appeared in the FTIR spectrum between 531 and 3260cm^{-1}. The bands 3260.14cm^{-1} and 2921.59cm^{-1} correspond to O-H stretching, 2855.77cm^{-1} corresponds to N-H stretching, 2237cm^{-1} corresponds to C≡N stretching, 1640.52cm^{-1}corresponds to C=N stretching, 1531.41cm^{-1} corresponds to N-O stretching; 1405.66cm^{-1} and 1335.55cm^{-1} correspond to O-H bending. 1240.83, 1166.35, 1117.55, and 1065.30cm^{-1} correspond to C-O stretch; 931.62cm^{-1} and 893.01cm^{-1} correspond to C=C bending; 659.35cm^{-1} and 609.30cm^{-1} correspond to C-Br stretch, and 531.89cm^{-1} correspond to C-I stretch (**Figure 4e**). Nanosizer and Zeta potential have been used to determine the size of the particles and their potential stability in the colloidal suspension. According to the previous published data, our synthesized AgNPs with a size distribution of 162.2nm, a polydispersity index (PDI) equal to 0.183, and particles carrying a charge of −5mV as clearly observed in **Figure 4f**, have relatively well-defined dimensions and high monodispersity in aqueous solutions. As observed from the analysis, the polydispersity index (PDI) value is lower than 0.7, which indicates the good quality of these synthesized AgNPs according to Khane and his co-workers [27].

3.4. Possible therapeutic applications of the produced biogenic AgNPs

Antimicrobial activity and Minimum Inhibitory Concentration (MIC) determination

Various concentrations of the biologically synthesized AgNPs (1000, 500, 250, 125, 62.5, and 31.25µg/100µl) using culture supernatants of *Halomonas* sp. FSSH were tested for their antimicrobial potential and showed significant antimicrobial activity against all tested pathogens. **Figure 5** depicts a microtiter plate while using an *in vitro* resazurin-based turbidometric (TB) assay containing the prepared AgNPs concentrations with the following pathogens: *E. coli (ATCC: 8739), K. pneumoniae* (ATCC: 13883), *P. aeruginosa* (ATCC: 15442), *V. parahemolyticus, E. faecalis* (ATCC: 29212), *S. aureus* (ATCC: 25923), and *B. subtilis* (ATCC: 6633). Wells for all tested bacteria treated with AgNPs remained as blue after an overnight incubation followed by a 4-h incubation with resazurin. In contrast, all wells in the growth control row (containing growth medium and bacteria) (3-10 D) of all tested bacteria had changed from blue to pink indicating their viability. The minimum inhibitory concentration (MIC) of the AgNPs against all tested pathogenic microbes was observed in the row before the last one (1-10 G) which was equivalent to 31.25 µg/100 µL.

19
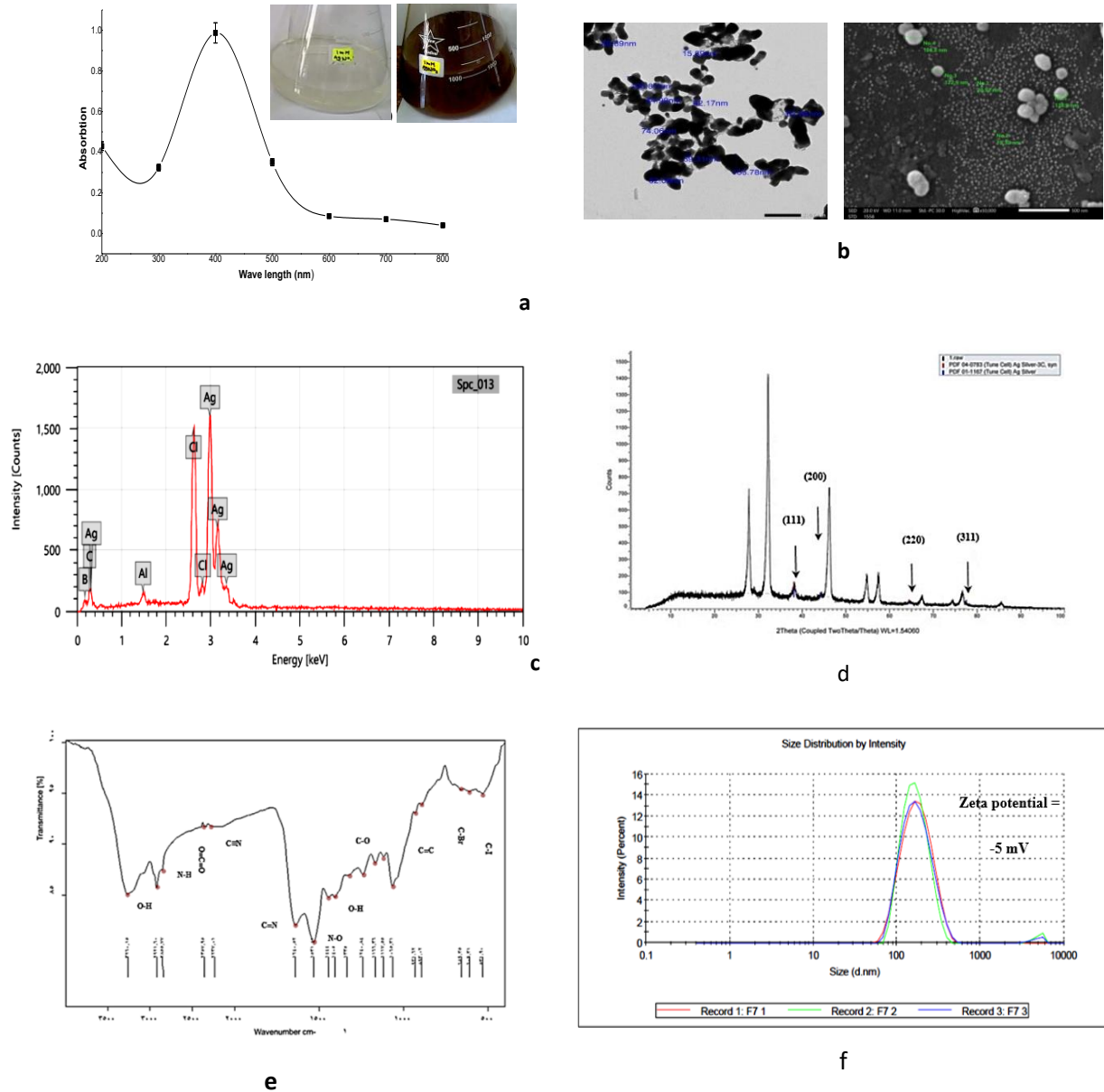
Figure 4. Characterization of AgNPs synthesised by *Halomonas* sp. FSSH cell-free supernatant using several analytical techniques: Ultraviolet-visible absorption spectrum (a); Images of TEM (left) and SEM (right) showing particle size and shape (b); EDX spectrum and micrograph (c); X-ray diffractogram (d). FTIR spectra (e) and Size distribution intensity graph (f)

3.5. Cytotoxicity of AgNPs against normal and malignant cells

To evaluate the cytotoxic effects of the synthesized AgNPs, normal rabbit leukocyte cells were subjected to several doses of AgNPs (1000, 500, 250, 125, 62.5, and 31.25 μg/ml) in a controlled experimental setting. The concentration of AgNPs has a direct correlation with the cytotoxicity seen in normal cells, as shown in **Figure 6a**. At a concentration of 1000 μg/mL, approximately 60% of the cells were found to survive. Throughout the study, the cytotoxicity of AgNPs was tested using an *in vitro* MTT assay on a human liver cancer cell line

20

(HepG2-HB-8065). AgNPs displayed cytotoxic effect in a dose-dependent manner. The cell line was treated with 31.25, 62.5, 125, 250, 500, and 1000 μg/mL AgNPs reduced cell viability to 30, 37, 45, 49, 56, and 65% with increasing concentrations, respectively whereas the cytotoxic action (IC_{50}) was observed at 419.671 μg/mL (**Figure 6b**). Consequently, AgNPs treatment induced apoptosis represented by changes in the morphology of cells shown by arrows, which was confirmed using the ZOE fluorescent cell imager (**Figure 6c**). Cells treated with 1000μg/ml AgNPs showed cytoplasmic shrinkage and loss of cell-to-cell contact.
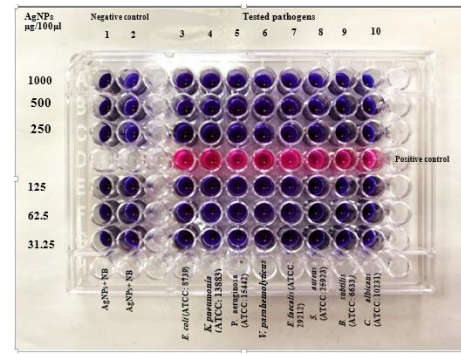
Figure 5. Resazurin Microtiter Assay (REMA) for Determining the Antimicrobial Activity and Minimal Inhibitory Concentration (MIC) of AgNPs against some tested pathogens.
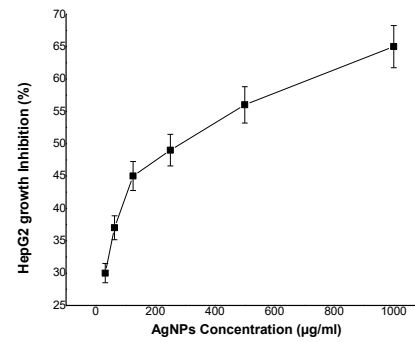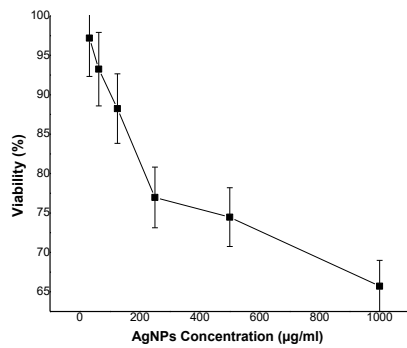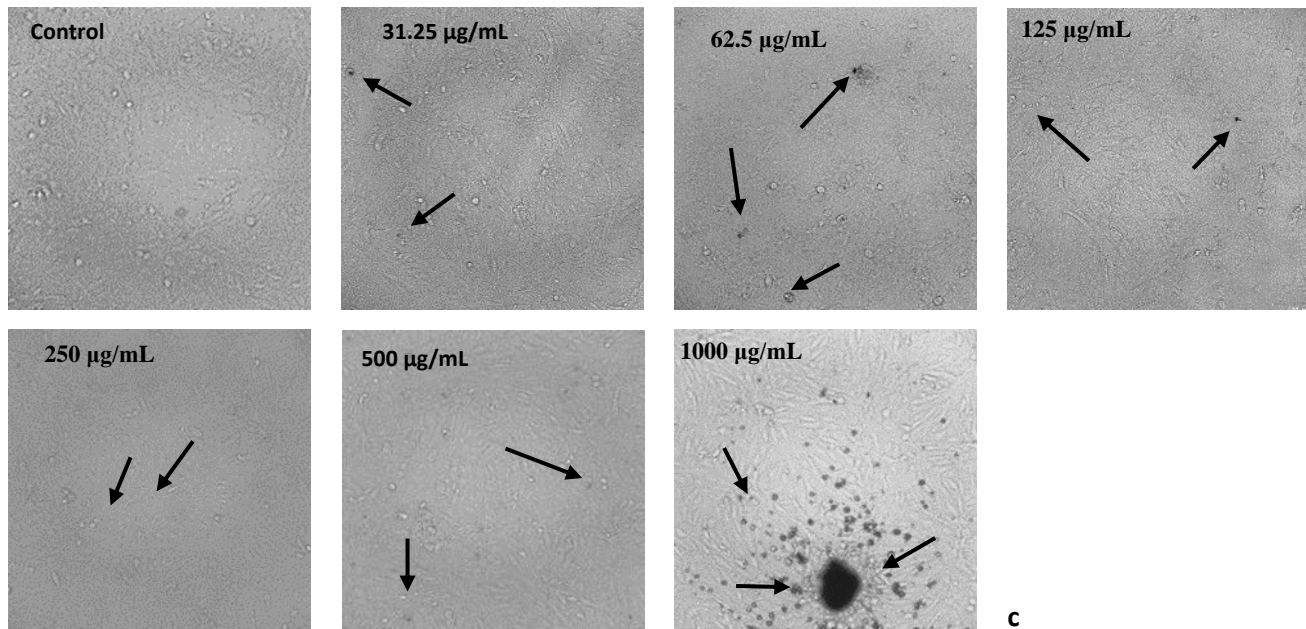
Figure 6. Cytotoxic effect of AgNPs, on the viability of normal rabbit leukocytic cells (a) growth inhibition of the HepG2 human cell line (b) Microscopic evaluation and morphological changes in HepG2 cells (shrinkage of cells is shown by an arrow) (c) at different concentration of 1000, 500, 250, 125, 62.5, and 31.25 μg/mL for 24h using MTT assay.

Wound healing activity of AgNPs

Silver nanoparticles' effect on wound healing was studied on a human epithelial cell line (WISH-CCL-25). A Human epithelial cell line was scratched and then treated with 100 µg/mL AgNPs. The quantitative analysis of wound healing involved measuring the initial wound gap size before treatment (control) along with healing towards wound closure (24h). As observed in **Figure 7**, AgNPs achieved 48% wound closure after 24h (**Figure 7a**). When compared to untreated cells, the presence of AgNPs accelerated wound reduction by 12% (**Figure 7b**). These findings show that AgNPs achieved 48% wound healing in 24 hours.

4. Discussion

Many bacterial taxa with silver ion (Ag^+) reduction activity towards AgNPs have been discovered, primarily in marine sediments [28]. Many reports have expressed concern about bacterial isolates producing AgNPs [18, 29]. The observed colour change from colourless to dark brown, as clearly observed by the two isolates (F8 and F9) throughout the study, thus serving as preliminary validation for the existence of silver nanoparticles as previously confirmed by Kumar and his co-workers [30]. In line with our results, isolate F8 had the highest surface plasmon resonance absorption peak at 400nm shown in **Figure 1**; Kharchenko and his co-workers [31] discovered that AgNPs have the highest surface plasmon resonance absorption peak at 400nm. In addition to Rai and his colleagues [32], who found a surface plasmon resonance peak at 420nm, confirmed the formation of the silver nanoparticles.

The most promising AgNPs-producing bacterium isolate F8 was morphologically characterized (**Figure 2**) as having a creamy colour, a regular margin, a convex shape, and a mucoid configuration. The cells appeared as Gram-negative rods occurring singly. In a sequential step, the molecular identification of the promising isolate (F8) was performed, and the sequence of the 16S rRNA gene in isolate F8 was 97% the same as the sequence of *Halomonas denitrificans* (NR_042491.1). The deposited sequence in GenBank OP716688 is designated as *Halomonas* sp. FSSH, and classified as a member of the genus *Halomonas*, family Halomonadaceae, order Oceanospirillaes, class γ-Proteobacteria, phylum Pseudomonadota. Previously, *Halomonas* was isolated from marine sediments and identified as *Halomonas piezotolerans* NBT06E8T, *Halomonas meridian, Halomonas maris* QX-1^T, *Halomonas profundi* MT13^T and MT32 strains [33-36], respectively. Most members of this genus are halotolerant, aerobic, Gram-stain-negative, rod-shaped, and non-sporulating [36]. *Halomonas* sp. FSSH showed a non-haemolytic reaction on blood agar, similar to the result reported by Woods and his co-workers [37]. *Halomonas* sp. FSSH showed non-lactose fermentation activity. This is different from what Yeo and his colleagues [38] found when they studied *Halomonas hamiltonii* and found that it didn't grow on MacConkey agar. *Halomonas* strain has been reported previously for the synthesis of silver nanoparticles. The study reported the ability of *Halomonas* strain for the synthesis of silver nanoparticles extracellularly through the bacterial mechanism used to reduce the colloidal silver ion to nanoparticles. With FTIR analysis, reducing protein compounds playing that role was revealed. In addition, complex compounds are also secreted by the bacterium in the supernatant that play role in stabilizing the nanoparticles [39].

Following synthesis, precise particle characterization is essential to overcome the safety issue and fully exploit the potential of any nanomaterial for humanity, nanomedicines, or the health care enterprise prior to application [40]. Therefore, several analytical techniques were applied to evaluate the bio-manufactured AgNPs. The UV/Vis spectrum of the colloidal solution of the synthesized AgNPs showed a strong, conspicuous, characteristic spectral absorption peak at 400 nm (**Figure 4a**), confirming its presence. The formation of the AgNPs during the reduction process is indicated by a change in the colour of the $AgNO_3$ from colourless to dark brown (**Figure 4a**) due to mutual vibrations of the free electrons in resonance with light waves, which are influenced by both the size and shape of the synthesized AgNPs. These results are in line with what was found by *Kocuria rhizophila* BR-1, *Lactobacillus gasseri*, and *Pseudomonas fluorescens* bacterial culture supernatants [30, 41, 36], respectively. According to TEM and SEM data analyses, the biosynthesized AgNPs are evenly distributed and have a spherical shape with an average size ranging from 15.69 to 133.78nm (**Figure 4b left**) and 18.30 to186.8nm (**Figure 4b right**), respectively. In accordance with the previously published data, Alsharif and his co-workers [42] synthesized spherical AgNPs with a size range of 6-50nm by *Bacillus cereus* A1-5, and Salem [43] fabricated spherical AgNPs with sizes ranging from 3 to 60nm using TEM analysis. Moreover, these findings agreed with those published by Saqib and his colleagues [44] and Rajendran and his co-workers [45], who reported the synthesis of spherical AgNPs using SEM analysis.

By using EDX analysis, it was possible to determine the elemental composition of the synthesized AgNPs. The strong absorption peak at 3keV in the metallic silver region was observed as confirmation for the AgNPs synthesis. A trace of elements in the form of peaks was detected together with silver ions by the EDX pattern (**Figure 4c**). These results confirmed the formation of the AgNPs as presented in the previous studies by Luhata and his co-workers [46] and Swamy and his colleagues [47]. The obtained diffraction pattern (XRD), the crystalline nature, and the calculated particle size (19.11 nm) using the Scherrer equation of AgNPs obtained and presented in **Figure 4d** were consistent with what Khane and his co-workers [27] and Loganathan and his co-workers [48] had reported, respectively. Also, similar data were obtained by El-Baradaei and his colleagues [49] when synthesized AgNPs from *Streptomyces* sp. RHS16.

The characteristic XRD peaks were centered at ~38.02◦, ~44.44◦ and ~64.51◦, 77.68◦, and 81.35◦ which could be induced by the following crystalline planes of silver: (111), (200), (220), (311), and (222), respectively. FTIR spectroscopy is a key method for producing molecular figures that can identify the functional group. Using this analysis, we can determine the chemical properties of the nanoparticles surfaces. As detected, various bands appeared in the FTIR spectrum between 531 and 3260 cm^{-1} (**Figure 4e**).

These functional groups show that bacterial biocomponents are present and acting as AgNPs capping and stabilizing agents. These biomolecules are in charge of the conversion of Ag^+ into AgNPs. This implies that the extract's constituent compounds

will stick to the nanoparticle's surface, encouraging capping and stability [50]. The functional groups that appeared in this analysis were in line with those previously published by El-Baradaei and his co-workers [49] who reported an array of absorbance bands from the FTIR spectral analysis of silver nanoparticles produced using *Streptomyces* sp. RHS16.

Using Nanosizer, our synthesized AgNPs with a size distribution of 162.2 nm, a polydispersity index (PDI) equal to 0.183, and particles carrying a charge of $-5mV$ as clearly observed in **Figure 4f**, have relatively well-defined dimensions and high monodispersity in aqueous solutions. As observed from the analysis, the polydispersity index (PDI) value is lower than 0.7, which indicates the good quality of these synthesized AgNPs according to Khane and his colleagues [27]. According to the previously published data, nanosizer and Zeta potential have been used to determine the size of the particles and their potential stability in the colloidal suspension. Therefore, nanoparticles with Z-potential quantities greater than +25 mV or less than -25 mV usually have high degrees of stability [51]. Using the zeta potential value, the amount of charge on the surface of the manufactured AgNPs was measured. The formation of different charge groups on the surface of the nanoparticles showed how stable they were in dispersion. The presence of negatively charged groups improves the stability and dispersion of AgNPs in aqueous solutions [52, 53].

Among the several promising nanomaterials, AgNPs seem to be potential antibacterial agents due to their large surface-to-volume ratios and crystallographic surface structure, as mentioned previously by Zhang and his co-workers [40]. Therefore, various concentrations of the biologically synthesized AgNPs using culture supernatants of *Halomonas* sp. FSSH were tested for their antimicrobial potential and showed significant antimicrobial activity against all tested pathogens. As clearly depicted in **Figure 5**, wells for all tested bacteria treated with AgNPs remained blue. In contrast, all wells in the growth control row of all tested bacteria had changed from blue to pink, indicating their viability. The minimum inhibitory concentration (MIC) of the AgNPs against all tested pathogenic microbes was equivalent to 31.25 μg/100μl. These findings contrast with those of Miranda and his co-workers [20], who discovered that their synthesised AgNPs were effective against *E. coli* but had no antibacterial activity against *S. aureus* and only weak antimicrobial activity against *Candida albicans*. According to Khane and his colleagues [27], they found that AgNPs have antimicrobial activity against *E. coli* ATCC 25922, *S. aureus* ATCC 25923, and *C. albicans*. Silver nanoparticles showed excellent zone inhibition against *Streptococcus pneumonia, Staphylococcus, Rhizopus stolonifer, and Aspergillus flavus* as reported by Oves and his co-workers [54]. The proposed mechanisms of AgNP-induced cell death were observed to be as previously mentioned by Zhang and his colleagues [40], in the case of *E. coli*, cell death was attributed to the release of reducing sugars and proteins. In addition, it has been shown that AgNPs had the capability to disrupt the integrity of bacterial membranes by inducing the formation of many pits and gaps. This suggests that AgNPs have the potential to impair the structural integrity of bacterial cell membranes.

The studied cytotoxic effects of the manufactured AgNPs on normal rabbit leukocyte cells indicated that the concentration of AgNPs has a direct correlation with the cytotoxicity seen in normal cells, as presented in **Figure 6a**. At a concentration of 1000μg/ml, approximately 60% of the cells were found to survive. The results of this study are consistent with those of a recent investigation by Elnady and his co-workers [55], which demonstrated that AgNPs did not cause cytotoxicity in healthy peripheral blood cells. In consistency with our findings and those of Naveed and his colleagues [56], this revealed a correlation between rising concentrations of hazardous AgNPs and reduced cell viability in U87-MG and HEK 293 cell lines. Throughout the study, the cytotoxicity of AgNPs was tested using an *in vitro* MTT assay on a human liver cancer cell line (HepG2-HB-8065). AgNPs displayed cytotoxic effects in a dose-dependent manner (**Figure 6b**). Consequently, AgNPs treatment induced apoptosis represented by changes in the morphology of cells shown by arrows, which was confirmed using the ZOE fluorescent cell imager (**Figure 6c**). Cells treated with 1000 μg/ml AgNPs showed cytoplasmic shrinkage and loss of cell-to-cell contact. According to Kamradgi and his co-workers [57], AgNPs showed anticancer activity of 99% at a concentration of 100 μg/mL and of 53 μg/ml while Sivakumar and his colleagues [58] reported that AgNPs have a 50% anticancer effect and a 100% inhibition at 100 μg/mL. Numerous attempts have been documented to elucidate the mechanism of action of nanoparticle cytotoxicity via the penetration of nanoparticles into mammalian cells either by phagocytosis or endocytosis. Another documented mechanism of action of nanoparticles is cytotoxicity via the manufacture of free radicals, which cause cellular disintegration leading to cell death [59].

The quantitative investigation of wound healing on a human epithelial cell line (WISH-CCL-25) involved measuring the initial wound gap size before treatment (control) with AgNPs along with healing towards wound closure (24h). The obtained results show that AgNPs achieved 48% wound healing in 24 hours (**Figure 7**). These findings contrasted with a recent study of *Ficus benghalensis* leaf extract at 1000 μg/mL, which produced AgNPs at a rate of 70.2% in 24 hours on HDFa cells [60]. This may suggest that some of the polyphenols and flavanols were involved in the synthesis of the AgNPs [61].

Finally, it is also worth mentioning to consider that the IC_{50} of particles against normal and HepG-2 cells are 1000 μg/mL and 419.6 μg/mL, respectively, which seems to have a SI of 2.3 that it means it is already selective. This could explain why it can have both growth-promoting action on the fibroblasts while inhibitory to the cancer cells, especially the wound healing effective concentration was 100 μg/mL.
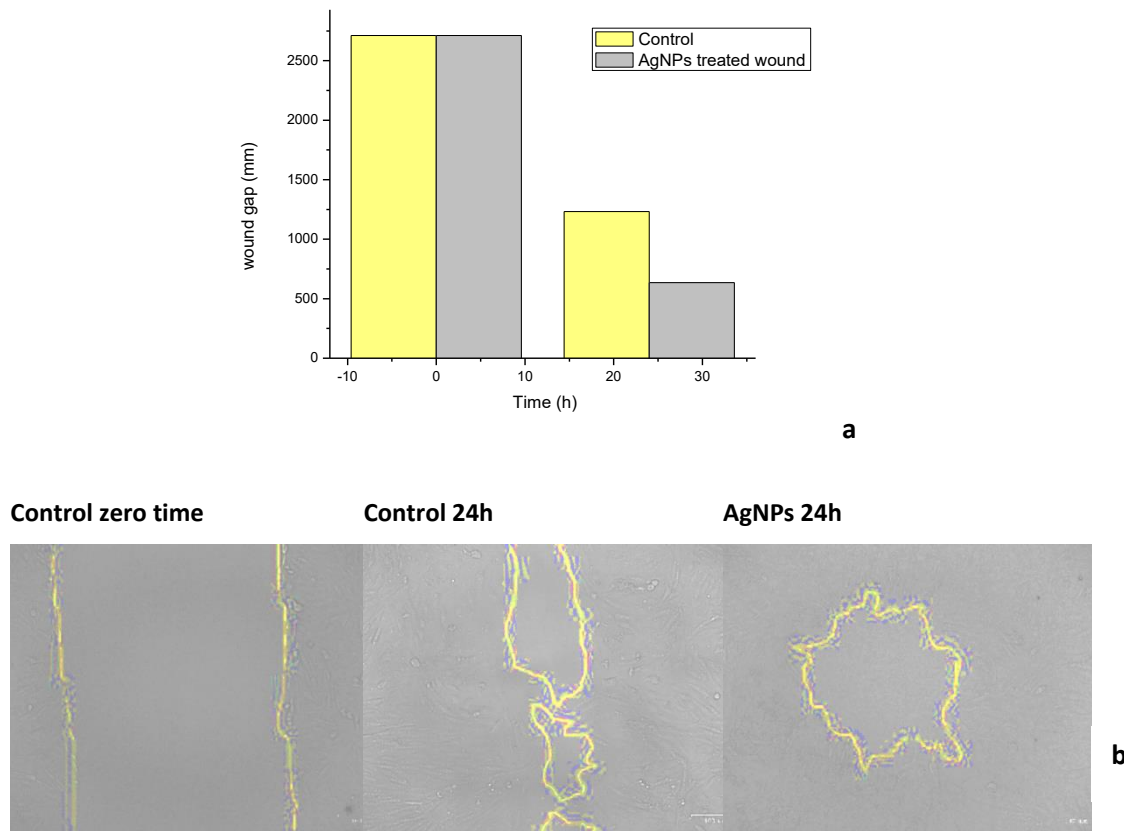
Figure 7. Wound healing effect of AgNPs on wound gap size in WISH cell line (a), morphological changes in the WISH cell line before and after exposure to AgNPs for 24h (b)

5. Conclusion

As a final conclusion at the end of this investigation, silver nanoparticles (AgNPs) were synthesized using a bacterial cell-free supernatant derived from *Halomonas* sp. The biological production of silver nanoparticles (AgNPs) via FSSH is a cost-effective, environmentally friendly, and secure process, presenting itself as a viable alternative to traditional chemical and physical procedures. The results of our study have provided confirmation that the use of a bacterial cell-free supernatant has the potential to serve as a viable approach for the production and the stabilisation of silver ions. The biosynthesized AgNPs showed strong antimicrobial effect, as demonstrated with the Resazurin assay. The overall findings reveal that biologically synthesized AgNPs stabilized by biomolecules showed no cytotoxic effect on normal rabbit leukocyte cells, suggesting their potential for safe utilization in various medical applications. Additionally, these AgNPs exhibit antiproliferative properties in the HepG2-HB-8065 liver cancer cell line by inducing apoptosis, suggesting their potential as a viable alternative for the treatment of human liver cancer. The experimental investigation included the use of silver nanoparticles (AgNPs) on a human epithelial cell line known as WISH-CCL-25, revealing their potential efficacy in promoting wound healing.

AUTHORS' CONTRIBUTION

F.M.H. proposed the research concept, conceived & conducted the experiments, and wrote the manuscript; S.S.A. conceived the idea and proposed the characterization plan of the research, analyzed and interpreted the data, performed the statistical analysis, participated in the practical work, and finally wrote, revised, and edited the manuscript in its final form; H.A.G. and S.A.S. conceived the research idea, analyzed the data, participated in the manuscript writing, and edited the manuscript.

COMPETING INTERESTS

The authors declare no competing interests.

References

[1] Khosravi, K.; Cruz, A.; Mozafari, M.; Moghadam, Z.; Ahmadi, N. Biosynthesis of Metal Nanoparticles by Probiotic Bacteria. Lett Appl NanoBioScience. 2019, 8, 619-626. doi:10.33263/LIANBS83.619626.

[2] Koul, B.; Poonia, A. K.; Yadav, D.; Jin, J. O. Microbe-Mediated Biosynthesis of Nanoparticles: Applications and Future Prospects. Biomolecules. 2021. 11, 886. doi:10.3390/biom11060886.

[3] Shafiq, T.; Uzair, M.; Iqbal, M. J.; Zafar, M.; Hussain, S. J.; Shah, S. A. A. Green Synthesis of Metallic Nanoparticles and their Potential in Bio-medical Applications. Nano Biomed Eng. 2021, 13.

[4] Zhu, D.; Sethupathy, S.; Sethupathy, S.; Gao, L.; Nawaz, M. Z.; Zhang, W.; Jiang, J.; Sun, J. Microbial Diversity and Community Structure in Deep-Sea Sediments of South Indian Ocean. Environ Sci Pollut Res. 2022, 29, 45793-45807. doi:10.1007/s11356-022-19157-3.

[5] Klębowski, B.; Depciuch, J.; Parlińska-Wojtan, M.; Baran, J. Applications of Noble Metal-Based Nanoparticles in Medicine. Int J Mol Sci. 2018, 19, 4031.

[6] Ansar, S.; Tabassum, H.; Aladwan, N. S. M.; Ali, M. N.; Almaarik, B.; AlMahrouqi, S.; Abudawood, M.; Banu, N.; Alsubki, R. Eco Friendly Silver Nanoparticles Synthesis by *Brassica oleracea* and its Antibacterial, Anticancer and Antioxidant Properties. Sci Rep. 2020, 10, 18564. doi:10.1038/s41598-020-74371-8.

[7] Ahmad, F.; Ashraf, N.; Ashraf, T.; Zhou, R. B.; Yin, D. C. Biological Synthesis of Metallic Nanoparticles (MNPs) by Plants and Microbes: Their Cellular Uptake, Biocompatibility, and Biomedical Applications. Appl Microbiol Biotechnol. 2019, 103, 2913-2935. doi:10.1007/s00253-019-09675-5.

[8] Sánchez-López, E.; Gomes, D.; Esteruelas, G.; Bonilla, L.; Lopez-Machado, A. L.; Galindo, R.; Cano, A.; Espina, M.; Ettcheto, M.; Camins, A.; Silva, A. M.; Durazzo, A.; Santini, A.; Garcia, M. L.; Souto, E. B. Metal-Based Nanoparticles as Antimicrobial Agents: An Overview. Nanomater. 2020, 10, 292.

[9] Boroumand, Z.; Golmakani, N.; Boroumand, S. Clinical Trials on Silver Nanoparticles for Wound Healing. Nanomed J. 2018, 5, 186-191.

[10] [Naraginti, S.; Kumari, P. L.; Das, R. K.; Sivakumar, A.; Patil, S. H.; Andhalkar, V. V. Amelioration of Excision Wounds by Topical Application of Green Synthesized, Formulated Silver and Gold Nanoparticles in Albino Wistar Rats. Mater Sci Eng C. 2016, 62, 293-300.

[11] Ramadan, Y.; El-Ashry, M. K.; Bahei-Eldin, I. A.; Soliman, A. S. E. D.; El-Nefiawy, N. E.; Zakaria, M. M. A. The Role of Silver Nanoparticles on Accelerating Healing of Skin Wound in Rats: Histological and Immunohistochemical Study. Ain Shams Med J. 2021, 72, 533-553.

[12] Hanaa, A. M. A.; Rasha, M. G.; Mohamed, R. H.; Khaled, M. Z.; Rasha, E. M. A. Identification of the Gastropod Snails and Shells Collected from Ain El-Sokhna Region, Red Sea, Egypt. Egyptian Journal of Aquatic Biology and Fisheries. 2021, 25, 101-117.

[13] Sandle, T. Gram's Stain: History and Explanation of the Fundamental Technique of Determinative Bacteriology. Inst Sci Technol J. 2004, 54, 3-4.

[14] Buxton, R. Blood Agar Plates and Hemolysis Protocols. American Society for Microbiology. 2005, 15, 1-9.

[15] Allen, M. E. MacConkey Agar Plates Protocols. American Society for Microbiology. 2005, 1-4.

[16] Gregersen, T. Rapid Method for Distinction of Gram-Negative from Gram-Positive Bacteria. Eur J Appl Microbiol. 1978, 5, 123-127.

[17] Sambrook, J.; Fritsch, E. F.; Maniatis, T. Molecular Cloning: A Laboratory Manual. Ed. 2., Cold spring harbor laboratory press, New yourk, 1989.

[18] Esmail, R.; Afshar, A.; Morteza, M.; Abolfazl, A.; Akhondi, E. Synthesis of Silver Nanoparticles with High Efficiency and Stability by Culture Supernatant of *Bacillus* ROM6 Isolated from Zarshouran Gold Mine and Evaluating its Antibacterial Effects. BMC Microbiol. 2022, 22, 97. doi:10.1186/s12866-022-02490-5.

[19] John, M.S.; Nagoth, J. A.; Ramasamy, K. P.; Mancini, A.; Giuli, G.; Miceli, C.; Pucciarelli, S. Synthesis of Bioactive Silver Nanoparticles Using New Bacterial Strains from an Antarctic Consortium. Mar. Drugs. 2022, 20, 558.

[20] Miranda, A.; Akpobolokemi, T.; Chung, E.; Ren, G.; Raimi-Abraham, B. T. pH Alteration in Plant-Mediated Green Synthesis and its Resultant Impact on Antimicrobial Properties of Silver Nanoparticles (AgNPs). Antibiot. 2022, 11, 1592.

[21] Gun, M.; Çaycı, Y.; Durupinar, B.; Coban, A. A. New Colorimetric Method for Rapid Detection of Antibiotic Resistance in *Escherichia coli* Isolates. Jundishapur J Microbiol. 2022, 14. doi:10.5812/jjm.119858.

[22] The, C. H.; Nazni, W. A.; Nurulhusna, A. H.; Norazah, A.; Lee, H. L. Determination of Antibacterial Activity and Minimum Inhibitory Concentration of Larval Extract of Fly Via Resazurin-Based Turbidometric Assay. BMC Microbiol. 2017, 17, 36. doi:10.1186/s12866-017-0936-3.

[23] Jabbar, S. A.; Twentyman, P. R.; Watson, J. V. The MTT Assay Underestimates the Growth Inhibitory Effects of Interferons. Br J Cancer. 1989, 60, 523-528. doi:10.1038/bjc.1989.306.

[24] Vinken, M., Rogiers, V. Protocols in in-vitro Hepatocyte Research. Eds., Humana Press, New York, 2015.

[25] Xue, Y.; Zhang, T.; Zhang, B.; Gong, F.; Huang, Y.; Tang, M. Cytotoxicity and Apoptosis Induced by Silver Nanoparticles in Human Liver HepG2 Cells in Different Dispersion Media. J App Toxicol. 2016, 36, 352-360. doi:10.1002/jat.3199.

[26] Martinotti, S.; Ranzato, E. Scratch Wound Healing Assay. Methods in Molecular Biology Clifton, N.J. 2020, 2109, 225-229. doi:10.1007/7651_2019_259.

[27] Khane, Y.; Benouis, K.; Albukhaty, S.; Sulaiman, G. M.; Abomughaid, M. M.; Al Ali, A.; Aouf, D.; Fenniche, F.; Khane, S.; Chaibi, W.; Henni, A.; Bouras, H. D.; Dizge, N. Green Synthesis of Silver Nanoparticles Using Aqueous *Citrus limon* Zest Extract: Characterization and Evaluation of their Antioxidant and Antimicrobial Properties. Nanomater. 2022, 12, 2013.

[28] Sivakumar, K.; Gopalakrishnan, K.; Sivasankar, P. Antibacterial Activity of a Novel Silver Nanoparticle Mediated by a Marine Actinobacterium Isolated from Marine Sediments. Eur J Mol Clin Med. 2021, 8, 4359-4368.

[29] [29] Saied, E.; Hashem, A. H.; Ali, O. M.; Selim, S.; Almuhayawi, M. S.; Elbahnasawy, M. A. Photocatalytic and Antimicrobial Activities of Biosynthesized Silver Nanoparticles Using *Cytobacillus firmus*. Life. 2022, 12, 1331.

[30] Kumar, M.; Upadhyay, L. S. B.; Kerketta, A.; Vasanth, D. Extracellular Synthesis of Silver Nanoparticles Using a Novel Bacterial Strain *Kocuria rhizophila* BR-1: Process Optimization and Evaluation of Antibacterial Activity. BioNanoScience. 2022, 12, 423-438. doi:10.1007/s12668-022-00968-0.

[31] Kharchenko, Y.; Lastovetska, L.; Maslak, V.; Sidorenko, M.; Vasylenko, V.; Shydlovska, O. Antibacterial Activity of Green Synthesised Silver Nanoparticles on *Saccharomyces cerevisiae*. Appl Sci. 2022, 12, 3466.

[32] Rai, R.; Vishwanathan, A.; Vijayakumar, B. Antibacterial Potential of Silver Nanoparticles Synthesized Using *Aspergillus hortai*. BioNanoScience. 2022, 13, 203–211.

[33] Qiu, X.; Cao, X.; Xu, G.; Wu, H.; Tang, X. *Halomonas maris* sp. nov., a Moderately Halophilic Bacterium Isolated from Sediment in the Southwest Indian Ocean. Arch Microbiol. 2021, 203, 3279-3285. doi:10.1007/s00203-021-02317-3.

[34] Saha, P.; Madliya, S.; Khare, A.; Subudhi, I.; Bhaskara Rao, K. V. Enzymatic Biodegradation, kinetic Study, and Detoxification of Reactive Red-195 by *Halomonas meridiana* Isolated from Marine Sediments of Andaman Sea, India. Environ Technol. 2023, 44, 2648-2667.

doi:10.1080/09593330.2022.2038276.

[35] Wang, J.; Xie, Z.; Liu, Y.; Yan, F.; Cao, J.; Liu, R.; Wang, L.; Wei, Y.; Fang, J. Complete Genome Sequence of a Multiple-Stress-Tolerant Bacterium *Halomonas piezotolerans* NBT06E8T Isolated from a

Deep-Sea Sediment Sample of the New Britain Trench. 3 Biotech. 2022, 12, 236. doi:10.1007/s13205-022-03283-3.

[36] Wang, F.; Wan, J. J.; Zhang, X. Y.; Xin, Y.; Sun, M. L.; Wang, P.; Zhang, W. P.; Tian, J. W.; Zhang, Y. Z.; Li, C. Y.; Fu, H. H. *Halomonas profundi* sp. nov., Isolated from Deep-Sea Sediment of the Mariana Trench. Int J Syst Evol Micr. 2022, 72, 005210.

[37] Woods, D.; Kozak, I.; O'Gara, F. Genome Analysis and Phenotypic Characterization of *Halomonas hibernica* Isolated from a Traditional Food Process with Novel Quorum Quenching and Catalase Activities. Microbiol. 2022, 168, 001238. doi:10.1099/mic.0.001238.

[38] Yeo, S. H.; Kwak, J. H.; Kim, Y. U.; Lee, J. S.; Kim, H. J.; Park, K. H.; Lee, J. S.; Ha, G, Y.; Lee, J. H.; Lee, J. Y.; Yoo, K. D. Peritoneal Dialysis-Related Peritonitis Due to *Halomonas hamiltonii*: A First Case Report. Medicine. 2016, 95, e5424. doi:10.1097/md.0000000000005424.

[39] Abdollahnia, M.; Makhdoumi, A.; Mashreghi, M.; Eshghi, H. Exploring the Potentials of Halophilic Prokaryotes from a Solar Saltern for Synthesizing Nanoparticles: The Case of Silver and Selenium. PLoS One. 2020, 15, e0229886. https://doi.org/10.1371/journal.pone.0229886.

[40] Zhang, X. F.; Liu, Z. G.; Shen, W.; Gurunathan, S. Silver Nanoparticles: Synthesis, Characterization, Properties, Applications, and Therapeutic Approaches. Int J Mol Sci. 2016, 17, 1534. doi: 10.3390/ijms17091534. PMID: 27649147; PMCID: PMC5037809.

[41] Sodimalla, T.; Yalavarthi, N. Biosynthesis of Silver Nanoparticles from *Pseudomonas fluorescens* and their Antifungal Activity Against *Aspergillus niger* and *Fusarium udum*. Ann Appl Biol. 2022, 181, 235-245.

[42] Alsharif, S. M.; Salem, S. S.; Abdel-Rahman, M. A.; Fouda, A.; Eid, A. M.; Hassan, S. E. D.; Awad, M. A.; Mohamed, A. A. Multifunctional Properties of Spherical Silver Nanoparticles Fabricated by Different Microbial Taxa. Heliyon. 2020, 6, e03943. ISSN 2405-8440, https://doi.org/10.1016/j.heliyon.2020.e03943.

[43] Salem, S. S.; Baker's Yeast-Mediated Silver Nanoparticles: Characterisation and Antimicrobial Biogenic Tool for Suppressing Pathogenic Microbes. BioNanoScience. 2022, 12, 1220–1229.

[44] Saqib, S.; Faryad, S.; Afridi, M. I.; Arshad, B.; Younas, M.; Naeem, M.; Zaman, W.; Ullah, F.; Nisar, M.; Ali, S.; Elgorban, A. M.; Syed, A.; Elansary, H. O.; Zin-El-Abedin,T. K. Bimetallic Assembled Silver Nanoparticles Impregnated in *Aspergillus fumigatus* Extract Damage the Bacterial Membrane Surface and Release Cellular Contents. Coat. 2022, 12, 1505.

[45] Rajendran, R.; Pullani, S.; Thavamurugan, S.; Radhika, R.; Lakshmi Prabha, A. Green Fabrication of

Silver Nanoparticles from Salvia Species Extracts: Characterization and Anticancer Activities Against A549 Human Lung Cancer Cell Line. Appl Nanosci. 2023, 13, 2571–2584.

[46] Luhata, L. P.; Chick, C. N.; Mori, N.; Tanaka, K.; Uchida, H.; Hayashita, T.; Usuki, T. Synthesis and Antioxidant Activity of Silver Nanoparticles Using the *Odontonema strictum* Leaf Extract. mol. 2022, 27, 3210.

[47] Swamy, P. S.; Bhat, M.; Nayaka, S. *Amycolatopsis* sp. Strain MN235945 Mediated Biosynthesis of Silver Nanoparticles: Characterization, Antimicrobial and Anticancer Activity Against HeLa and MCF-7 Cell Lines. Indian J Pharm Sci. 2022, 84, 1178-1188.

[48] Loganathan, S.; Selvam, K.; Shivakumar, M. S.; Senthil-Nathan, S.; Vasantha-Srinivasan, P.; Prakash, D. G.; Karthi, S.; Al-Misned, F.; Mahboob, S.; Abdel-Megeed, A.; Ghaith, A.; Krutmuang, P. Photosynthesis of Silver Nanoparticle (AgNPs) Using Aqueous Leaf Extract of *Knoxia sumatrensis* (Retz.) DC. and their Multi-Potent Biological Activity: an Eco-Friendly Approach. Mol. 2022, 27, 7854.

[49] El Baradaei, R. F.; Abouelkheir, S. S.; Ghozlan, H. A.; Sabry, S. A. Characterization and Antimicrobial Activity of AgNPs Synthesized by *Streptomyces* sp. RHS16 Against Fish Pathogens. J Pharm Biol Sci (IOSR-JPBS). 2018, 13, 59-67.

[50] Rodríguez-Félix, F.; López-Cota, A. G.; Moreno-Vásquez, M. J.; Graciano-Verdugo, A. Z.; Quintero-Reyes, I. E.; Del-Toro-Sánchez, C. L.; Tapia-Hernández, J. A. Sustainable-Green Synthesis of Silver Nanoparticles Using Safflower (*Carthamus tinctorius*) Waste Extract and its Antibacterial Activity. Heliyon. 2021, 7, e06923. doi:10.1016/j.heliyon.2021.e06923.

[51] Taghavizadeh-Yazdi, M. E.; Darroudi, M.; Amiri, M. S.; Zarrinfar, H.; Hosseini, H. A.; Mashreghi, M.; Mozafarri, H.; Ghorbani, A.; Mousavi, S. H. Antimycobacterial, Anticancer, Antioxidant and Photocatalytic Activity of Biosynthesized Silver Nanoparticles Using Berberis Integerrima. Iran J Sci Technol Trans A Sci. 2022, 46, 1-11.

[52] Shu, M.; He, F.; Li, Z.; Zhu, X.; Ma, Y.; Zhou, Z.; Yang, Z.; Gao, F.; Zeng, M. Biosynthesis and Antibacterial Activity of Silver Nanoparticles Using Yeast Extract as Reducing and Capping Agents. Nanoscale Res Lett. 2020, 15, 1-9.

[53] Muddassir, M.; Raza, A.; Munir, S.; Basirat, A.; Ahmed, M.; Butt, M. S.; Dar, O. A.; Ahmed, S. S.; Shamim, S.; Naqvi, S. Z. H. Antibacterial Efficacy of Silver Nanoparticles (AgNPs) Against Metallo-β-Lactamase and Extended Spectrum β-Lactamase Producing Clinically Procured Isolates of *Pseudomonas aeruginosa*. Sci Rep. 2022, 12, 20685. doi:10.1038/s41598-022-24531-9.

[54] Oves, M.; Rauf, M. A.; Aslam, M.; Qari, H. A.; Sonbo, H.; Ahmad, I.; Zaman, G. S.; Saeed, M. Green Synthesis of Silver Nanoparticles by *Conocarpus Lancifolius* Plant Extract and their Antimicrobial and Anticancer Activities. Saudi J Biol Sci. 2022, 29, 460-471.

[55] Elnady, A.; Sorour, N. M.; Abbas, R. Characterization, Cytotoxicity, and Genotoxicity Properties of Novel Biomediated Nanosized-Silver by Egyptian *Streptomyces roseolus* for Safe Antimicrobial Applications. World J Microbiol Biotechnol. 2022, 38, 47.

[56] Naveed, M.; Batool, H.; Rehman, S. u.; Javed, A.; Makhdoom, S. I.; Aziz, T.; Mohamed, A. A.; Sameeh, M. Y.; Alruways, M. W.; Dablool, A. S.; Almalki, A. A.; Alamri, A. S.; Alhomrani, M. Characterization and Evaluation of the Antioxidant, Antidiabetic, Anti-inflammatory, and Cytotoxic Activities of Silver Nanoparticles Synthesized Using *Brachychiton populneus* Leaf Extract. Processes. 2022, 10, 1521.

[57] Kamradgi, S.; Babanagare, S.; Gunagambhire, V. Characterization of *Talaromyces islandicus*–Mediated Silver Nanoparticles and Evaluation of their Antibacterial and Anticancer Potential. Microsc Res Tech. 2022, 85, 1825-1836.

[58] Sivakumar, M.; Surendar, S.; Jayakumar, M.; Seedevi, P.; Sivasankar, P.; Ravikumar, M.; Anbazhagan, M.; Murugan, T.; Siddiqui, S. S.; Loganathan, S. *Parthenium hysterophorus* Mediated Synthesis of Silver Nanoparticles and its Evaluation of Antibacterial and Antineoplastic Activity to Combat Liver Cancer Cells. J Clust Sci. 2021, 32, 167-177.

[59] Hamouda, R. A.; Hussein, M. H.; Abo-elmagd, R. A.; Bawazir, S. S. Synthesis and Biological Characterization of Silver Nanoparticles Derived from the Cyanobacterium *Oscillatoria limnetica*. Sci Rep. 2019, 9, 13071. https://doi.org/10.1038/s41598-019-49444-y.

[60] Lu, H.; Liu, S.; Zhang, Y. Development of Novel Green Synthesized Silver Nanoparticles with Superior Antibacterial and Wound Healing Properties in Nursing Care After Rectal Surgery. J Inorg Organomet Polym Mater. 2022, 32, 773-780. doi:10.1007/s10904-022-02223-1.

[61] Tyavambiza, C.; Meyer, M.; Wusu, A. D.; Madiehe, A. M.; Meyer, S. The Antioxidant and *in vitro* Wound Healing Activity of *Cotyledon orbiculata* Aqueous Extract and the Synthesized Biogenic Silver Nanoparticles. Int J Mol Sci. 2022, 23, 16094.